Journal of Power Sources 455 (2020) 227991

Contents lists available at ScienceDirect

Journal of Power Sources

journal homepage: www.elsevier.com/locate/jpowsour

Lifting the energy density of lithium ion batteries using graphite film current collectors

Qian Wu [a,1], Jinlong Yang [c,1], Yuwei Zhao [a], Rongguo Song [b], Zhe Wang [b], Zhe Huang [a], Mingyuan Shi [a], Yusheng Ye [c], Daping He [b,*], Shichun Mu [a,**]

[a] State Key Laboratory of Advanced Technology for Materials Synthesis and Processing, Wuhan University of Technology, Wuhan, 430070, China
[b] Hubei Engineering Research Center of RF-Microwave Technology and Application, School of Science, Wuhan University of Technology, Wuhan, 430070, China
[c] Department of Materials Science and Engineering, Stanford University, Stanford, CA, 94305, USA

HIGHLIGHTS

- Super light-weight graphite film is fabricated in large scale.
- It has ultrahigh electrical/heat conductivity, flexibility and mechanical features.
- It can replace traditional metal foil as current collector in lithium ion batteries.
- It shows a great enhancement in rate property, cycle durability and energy density.
- It has stable output in flexible pouch cells during various bending and distorting.

GRAPHICAL ABSTRACT

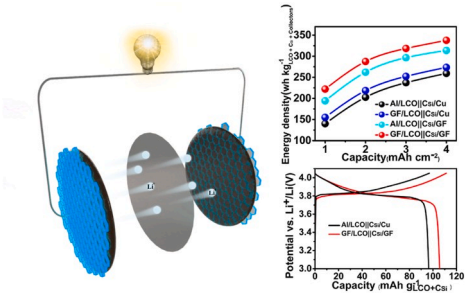

ARTICLE INFO

Keywords:
Light-weight
Flexibility
Graphite film
Current collector
Lithium ion batteries

ABSTRACT

Lightweight and highly conductive flexible films are attractive for a wide range of devices, especially replacing heavy metal-based current collectors, which can greatly reduce the weight of inactive materials in batteries and further enhance the energy density of energy storage devices. In this study, we first report a graphite film (GF) with ultralight weight (3.44 mg cm^{-2}), high electrical conductivity (up to $1.07*10^6$ S m^{-1}), fast heat transport and excellent anti-wrinkle (300 times folding) properties. When used as current collector of half-cells, GF can enhance the rate property and long cycle durability of Li-ion batteries (LIBs) by reducing the contact resistance between active materials and current collector and buffering the stress during charge/discharge. By further employing GF current collectors to completely replace the Al and Cu foils at both sides of full cells, the electrode energy density of $LiCoO_2$||Csi cell (4 mAh cm^{-2}) is greatly boosted from 260 Wh kg^{-1} to 332 Wh kg^{-1}. Moreover, such a GF film with excellent wrinkle resistance enables it to be used in flexible pouch cells with stable power output during various bending and distorting.

* Corresponding author.
** Corresponding author.
E-mail addresses: hedaping@whut.edu.cn (D. He), msc@whut.edu.cn (S. Mu).
[1] These authors contributed equally to this work.

https://doi.org/10.1016/j.jpowsour.2020.227991
Received 31 December 2019; Received in revised form 24 February 2020; Accepted 2 March 2020
Available online 9 March 2020
0378-7753/

1. Introduction

Due to the miniaturization and lightweight of portable electronic equipment, as well as the booming of battery electric vehicles (BEVs) and power storage devices, demands about the higher energy density of lithium-ion batteries (LIBs) are growing [1,2]. For enhancing energy density, finding or synthesizing new active and high-density materials are common methods [3–13]. In addition, reducing the weight of the battery is also an important perspective to solve this challenge. Having no effect on the capacity, but the proportion of traditional metal current collectors commonly used in LIBs, such as copper (Cu) and aluminum (Al) foils, is 15%–35% of total weight of the battery [14]. Thus, several attempts have been made to design novel current collectors for elevating the energy density of LIBs. For instance, the current collectors with rough surface or metal nanostructures (such as nanoneedles, nanowires, nanoporous and nanorods) have been explored [15–21], which not only ensure their high electrical conductivity, but also increase their contact strength with electrode materials. However, the mechanical inferiority and corrosion of metal current collectors also remain substantially, and the metal is still heavy to fail to promote the energy density of the battery. Consequently, the demand for thin, lightweight current collectors with high conductivity, strong mechanics and chemical stability is exceptionally urgent.

Owing to carbon materials exhibit lower density, superior flexibility and chemical stability than metals, a series of carbon current collectors with high specific surface area have been developed, such as reduced graphene oxide films, carbon nanotube films and graphene coated films [22–26], to improve the cycle stability and energy density. Among these carbon materials, most reports are focusing on reduced graphene oxide (RGO) films, but it is very hard to get large-area GO sheets due to unavoidable breaking of GO sheets during oxidation and exfoliate graphite processes, resulting in high contact resistance in the resultant RGO films [27]. Simultaneously, a huge challenge is to obtain high purity and pristine graphene by RGO, as defects and functional groups in partial reduced RGO will largely hinder carrier transport [22]. The highest electrical conductivity reported in RGO nanostructures [22,28–34] is typically less than 10^6 S m^{-1}, which make them very hard to meet the requirements of LIBs and difficult to get practical applications.

Enlightened by fabricating flexible graphite films with certain polymer precursors reported in 1990s [35], here we developed flexible lightweight graphite film (GF) by direct carbonization and graphitization of polyimide films (PI). It was the extraordinary planar conductivity and low surface sheet resistance brought from the high planar oriented structure that GF possesses ultrahigh electrical conductivity of $1.07*10^6$ S m^{-1}. When used as current collector for cathodes (commercial $LiCoO_2$ and $LiFePO_4$) in LIBs, GF exhibited higher rate performance than Al collector. When used as current collector for anode (commercial Csi), GF demonstrated higher capacity and better cycle stability compared to that used Cu foils. As a result, the energy densities of half and full-cell (LiC_OO_2||Csi) were greatly improved by replacing the current collectors with GF. In addition, flexible pouch cells were assembled by applying GF as current collector and exhibited stable power output even suffered continuous bending and distorting.

2. Experimental

2.1. Materials

Commercial $LiCoO_2$ and $LiFePO_4$ cathodes were obtained from HF-KEJING Co., Ltd, Csi anode was purchased from BTR New Energy Materials Inc. Electrolyte solutions were purchased from Shenzhen CAP-CHEM Technology Co., Ltd, PI Film (53 μm) was purchased from Wuxi Chengyi education technology Co., Ltd.

2.2. Characterization

SEM analysis was conducted on a JEOL-7100F scanning electron microscope at 20.0 kV. HRTEM analysis was conducted by the use of a JEM-2100F high-resolution transmission electron microscopy. Raman spectra were recorded on a Spectra-Physics Model 2025 argon ion laser with 457.9 nm laser. XRD was carried out on a Polycrystal PANalytical X'Pert Pro installations with Cu Ka radiation. XPS spectra were recorded on an ESCALAB 250Xi photoelectron spectrometer with Al Ka radiation as the X-ray source set. Electrical conductivity was measured by Four-Point Probes RTS-9. Infrared thermal was measured by using Fluke Ti400 thermal imagers. Volume electrical resistance was taken out by the use of a digital multi-meter (Agilent U1242B).

2.3. Electrochemical measurements

Electrochemical properties were evaluated using CR2032 Coin cells assembled in an argon-filled glove box ($H_2O < 0.1$ p.p.m. and $O_2 < 0.1$ p.p.m.). A cathode slurry composed of lithium iron phosphate ($LiFePO_4$, LFP) or lithium cobalt oxides ($LiCoO_2$, LCO), acetylene black, and binder (polyvinylidene fluoride, PVDF) with a mass ratio of 8:1:1 dissolve in *N*-methyl-2-pyrrolidone (NMP) was prepared, cast onto Al foil and as prepared GF, then dried in a vacuum oven for 10 h at 100 °C to obtain the cathode electrode. Anode electrodes were made by pitching a mix slurry of 80 wt% silicon carbon, 10 wt% acetylene black and 10 wt% binder mixture (styrene butadiene rubber, SBR and Carboxymethyl Cellulose, CMC) on Cu foil and as prepared GF at 100 °C under vacuum for 10 h.

For the half-cell test, working electrodes were gained by punching the dried electrode films, and Li metal as the reference and counter electrode. For the full-cell test, positive and negative electrodes both were electrode films. Working electrodes and reference electrodes were electronically separated by Celgard 2400 polypropylene saturated with Type LBE502A1 electrolyte solution for cathode coin cell and Type LBC3401A4 electrolyte solution for anode half-cell and full-cell. The cells were first cycled at 25 μA for three cycles for cell activation. The electrochemical performances [36] were obtained using the NEWARE battery-test system (Wuhan, China) in the potential range of 2.0–4.1 V (*vs.* Li/Li^+) for $LiFePO_4$ coin cells, 3.0–4.35 V (*vs.* Li/Li^+) for LiC_OO_2 coin cells, 0.01–3.0 V (*vs.* Li/Li^+) for Csi coin cells and 2.7–4.05 V (*vs.* Li/Li^+) for LiC_OO_2||Csi full-cells under room temperature.

3. Results and discussion

The GF of this work was fabricated via a two-step heat treatment process (Fig. 1a) carried out in vacuum and Ar atmosphere, respectively. Firstly, polyimide (PI) film was employed and slowly heated to 1300 °C, and carbonized for 6 h to generate a disordered structural carbon film. Then, the carbonized structure was burned at 2850 °C to hybridize the graphite structure with the fully formed C–C sp^2. Lastly, rolling technology was performed to further obtain highly oriented GF accompanied with a densely structure [37,38]. We can get several meters of GF at one time, demonstrating it can be produced in large-scale industrial preparation (Fig. 1b). Next, a series of representations were performed to analyze the structure of GF, including SEM, TEM, XRD, XPS and Raman. Firstly, the cross-sectional image represents that this extremely thin graphite film is about 17 μm (Fig. 1c) and stacked orderly of graphene layers (Fig. 1d), which means there is a structure with a highly in-plane orientation and an arrangement of aromatic segments parallel to the base surface. Then, the SEM image (Fig. 1e) shows the surface of GF seems to be rough. The HRTEM image (Fig. 1f) further shows GF possesses a clear sp^2 graphitic structure completely transferred from PI, agreed well with selected area diffraction (SAED) pattern, confirming that the graphene monolayer is the basic assembly layer structure in GF.

The Raman spectrum (Fig. 1g) of GF shows the ratio (I_D/I_G) is 0.17, indicating minims disorder degree of the graphitic structure [39]. The

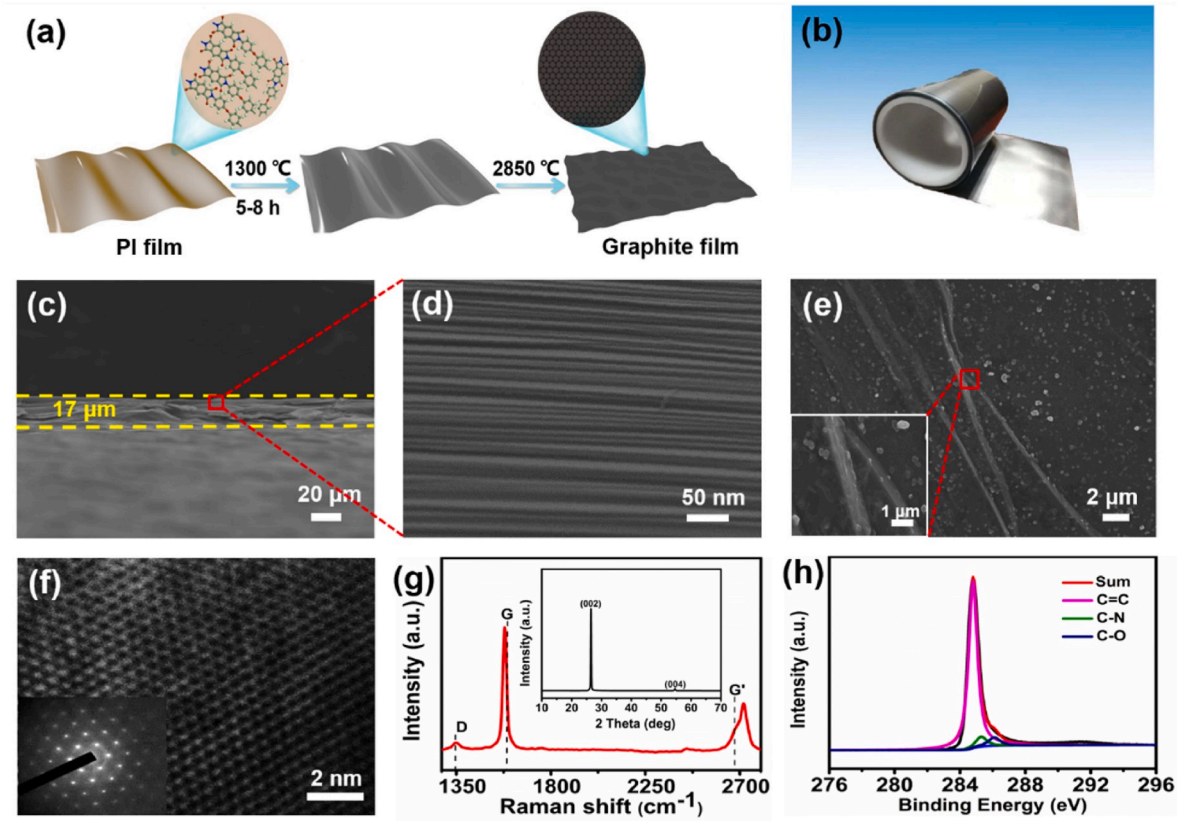

Fig. 1. (a) Scheme of the fabrication process, (b) photograph of a large scale rolled GF, (c, d) SEM images showing the cross-section of GF, (e) Surface morphology of Graphite film (inset is partially enlarged image of (e)), (f) HRTEM image of exfoliated GF (inset is SAED pattern of (f)), (g) Raman spectra of GF (inset is XRD pattern of GF), (h) XPS spectra corresponding to C 1s region for the GF.

XRD pattern shows the sharp and strong (002) and (004) diffraction peaks of GF. The apparent characteristic graphite peak is located around 26.5°, corresponding to the interlayer spacing is 0.33 nm, which indicates that the regular packing of graphene layers possesses longer correlation length. The high graphitization of GF also can be interpreted by the relatively intense diffraction peak (004). The high-resolution XPS spectrum of GF (Fig. 1h and Fig. S1) shows three peaks located at 284.7, 285.5 and 286.9 ev for C═C, C–N and C–O, respectively [40]. The high intensity of the C═C peak indicates the high graphitization of GF [41, 42], which is very consistent with the XRD image. We suggest that the

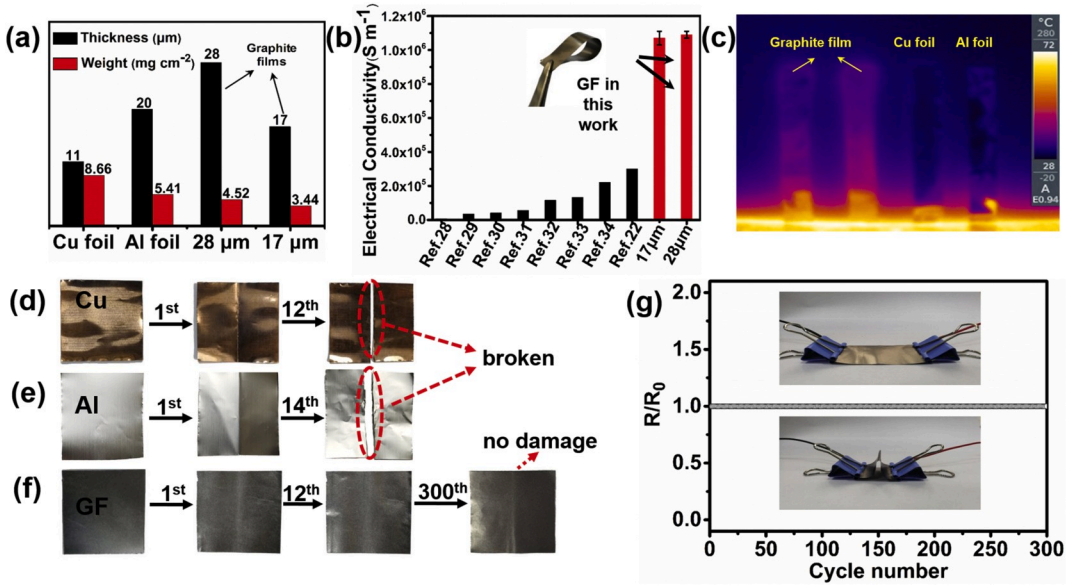

Fig. 2. (a) Comparison of thickness and mass of GF current collectors with commercial Cu and Al foils, (b) electronic conductivities of GF compared with the reported Graphene film by literatures, inset is the digital photograph of GF, (c) infrared thermal photographs of GF, Cu and Al foils, (d–f) digital photographs of (d) Cu, (e) Al and (f) GF current collectors after folding different times, (g) electrical conductivity change ratio before and after folding 300 times.

ordered graphite structure with high density and low defect is favorable to improving the electrochemical performance and mechanical property.

To investigate the unique physical properties of GF, we firstly demonstrate the advantages of GF in thickness and weight aspects, which play huge roles in practical applications in LIBs. The weight of GF with 17 μm of thickness is 3.44 mg cm^{-2}, which is six tenths of the weight of Al foil with 20 μm of thickness, and less than that of Cu foil with 11 μm of thickness (Fig. 2a). Therefore, we believe the light-weight GF current density can improve the energy density of LIBs.

In addition, we compared the electrical conductivity of previously reported graphene and RGO nanostructures [22,28–34] with metal foil (Fig. S2) and our GF (Fig. 2b). It can be clearly seen that GF have the highest electrical conductivity as high as $1.09*10^6$ S m^{-1} with thickness of 28 μm, which is much higher than literature reported. When the thickness decreases to 17 μm, the electrical conductivity of GF can maintain at $1.07*10^6$ S m^{-1}. The high electrical conductivity is benefit to improve the electrochemical performance of LIBs.

In a real battery, localized high temperature can cause internal shorting, which would further elevate the temperature and increase the risk of thermal runaway [43]. As visually demonstrated by the infrared thermal photographs (Fig. 2c), the thermal transfer rate of GF is obviously faster than that of the Cu and Al foils. Therefore, we conclude that GF can homogenize the heat produced by the stripping-plating process of lithium and make the battery safer.

We further analyzed the bending resistance of current collectors. Cu and Al foils (Fig. 2d and e) were broken after only 12 and 14 times bending, respectively, while GF kept consistent even after 300 times folding (Fig. 2f). The volume resistance before and after folding (Fig. 2g) was tested to prove steady electrical conductivity of GF. No difference in electrical resistance can be observed even after 300 times folding, demonstrating GF is prominent stable. Note that, both the extremely high electrical conductivity and good thermal property, as well the flexibility make GF potential to be a highly efficient current collector for LIBs.

To verify GF is alternative to metal current collectors, half-cells with GF as current collector were assembled with the Li metal as the anode and the commercial $LiCoO_2$ as cathode. For comparison, cells with Al foil were also tested. Observing from the initial two cycles charge/discharge curves (Fig. 3a) of commercial $LiCoO_2$ at a current density of 0.1 C (1.0 C = 150 mA g^{-1}), the initial coulombic efficiency of $LiCoO_2$/GF cell is 92.12%, higher than that of $LiCoO_2$/Al cell (88.32%). Meanwhile, the charging platform of $LiCoO_2$/GF cell is lower than that of $LiCoO_2$/Al cell, indicating smaller polarization for the GF current collector. Then, in the following cycles the discharge capacity stabilizes at 145.69 mAh g^{-1} (Fig. 3b). The SEM images in the insertion diagram shows no structure destruction was observed from the entire electrode after the cycle, which demonstrates that during lithium stripping-plating process, good contacts can be maintained between the GF and electrode. The rate property (Fig. 3c) shows that the specific capacities of the two cells are close at low rates from 0.2 to 1.0 C, but with the current density further increases, the difference in the capacity becomes extremely obvious. $LiCoO_2$/GF cell shows more steady discharge capacities, even though at high cycling rates. The capacities of $LiCoO_2$/GF at high rate of 2.0 and 5.0 C are 119.72 and 107.92 mAh g^{-1}, respectively, whereas the capacities for $LiCoO_2$/Al cell decreases to 112.52 mAh g^{-1} at 2.0 C and further quickly decrease to 91.76 mAh g^{-1} at 5.0 C. When the current density is back from 5.0 C to 2.0 C, $LiCoO_2$/GF cell can recover to its initial capacity, indicating the super-stability of electrode materials and GF at large current densities.

To clarify the mechanism for the high rate performance of $LiCoO_2$/GF, we analyzed the electrochemical impedance spectra (EIS) of batteries (Fig. 3d). The impedance plot consists of a depressed semicircle. The ohmic resistance (Rs), standing for inner contact resistance of cells, can be estimated from the high frequency intercept on the Z′ axis. The charge transfer resistor (Rct) corresponds to a semicircle in the mid-frequency range [44,45]. In this work, the Rs values (1.5 Ω) of $LiCoO_2$/GF cell is lower than that (2.3 Ω) of $LiCoO_2$/Al. Two factors contribute to the decrease in contact impedance: one is rough surface of GF (Fig. 1e) provides larger contact area between the electrode and current collectors; Second is the elimination of the schottky barrier. For traditional $LiCoO_2$/Al cell, the work functions of metallic Al (−4.25 eV) [46,47] is different from that of graphitized carbon black (−4.6 eV) [48,49] within the electrode, resulting in some of the electronic transmission is blocked, while in $LiCoO_2$/GF cell, there is no difference in work function between GF and graphitized conductive agent, ensuring the smooth transport of electrons. In addition, the Rct value (60 Ω) of $LiCoO_2$/GF cell is also lower than that (72 Ω) of $LiCoO_2$/Al,

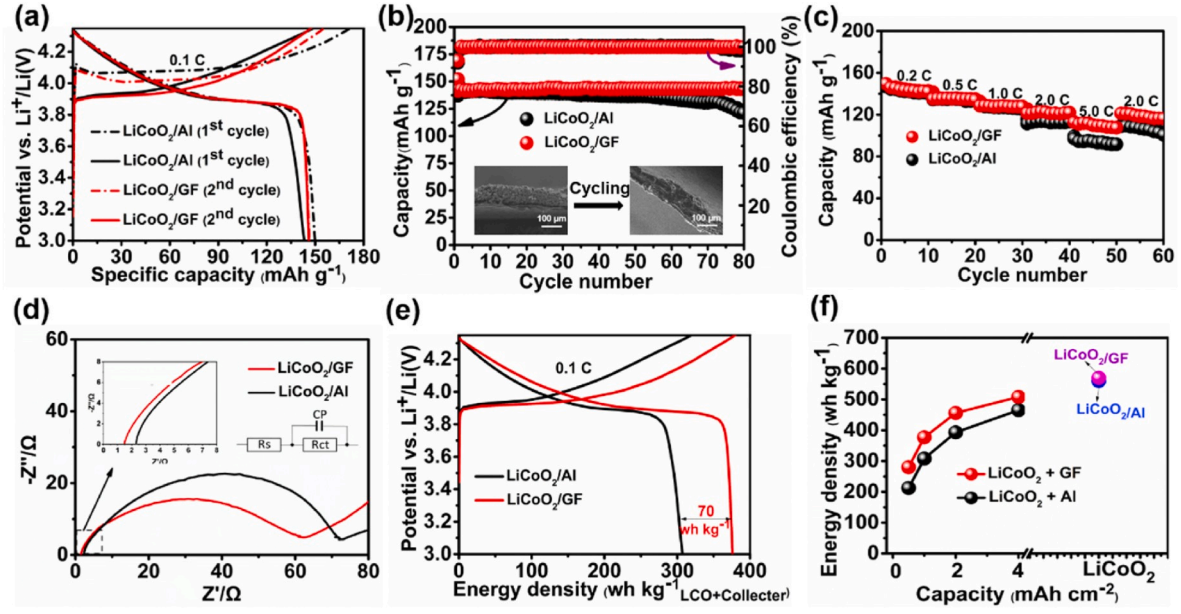

Fig. 3. (a) Initial 2 cycled discharge/charge curves at 0.1 C, (b) cycling performance at 0.2 C, (c) rate capability between 0.2 C and 5.0 C, (d) impedances and (e) electrode energy density of the commercial $LiCoO_2$ on Al foil and GF current collectors, (f) electrode energy density change with increasing areal capacity for different current collectors. Insert images of (b) are cross section SEM images of the electrode before and after cycling.

demonstrating a larger exchange current density (i = RT/nFRct, T is absolute temperature (298.15 K), F is Faraday constant, R is gas constant and n is the number of electrons per reaction species) [50], which is the main contribution to high rate performance of $LiCoO_2$/GF cell.

We further evaluated the advantage of GF current collector in improving the energy density. We firstly designed two half-cells (Li||$LiCoO_2$/Al and Li||$LiCoO_2$/GF) with 1.0 mAh cm^{-2} (Fig. S3). It can be incarnated that the electrode energy density of Li||$LiCoO_2$/GF cell reaches 375 Wh kg^{-1}, which is about 70 Wh kg^{-1} higher than that of Li||$LiCoO_2$/Al cell (Fig. 3e). Furthermore, we illustrated the relationship of area capacity and electrode energy density on different current collectors (Fig. 3f). As the weight of current collectors is considered, the electrode energy density of the $LiCoO_2$/GF is obviously elevated. When the area capacity increases to 4 mAh cm^{-2}, the electrode energy density of the $LiCoO_2$/GF battery reaches 500 Wh kg^{-1}, while the electrode energy density of the $LiCoO_2$/Al battery is only 460 Wh kg^{-1}. In addition, the advantages of GF as current collector were further confirmed when the commercial $LiFePO_4$ was used (Figs. S4–S8). Therefore, we conclude that the GF current collector can improve the cycle life, increase the rate capacity and energy density of cathodes for LIBs.

We further explored the application of GF as the current collector of anode. The commercial Csi anode material with nominal capacity of 450 mAh g^{-1} was coated on the GF and Cu foil, respectively, and then Li||Csi/GF and Li||Csi/Cu half-cells were assembled. The area capacities of such half-cells were designed as 1.0 mAh cm^{-2}. Observing from the initial two discharge/charge curves of the two half-cells at 0.1C (Fig. 4a), the 1st discharge capacity and coulombic efficiency of Csi/GF cell are ~1.41 mAh cm^{-2} and 83.31%, respectively, both of which are larger than that of Csi/Cu cell (1.16 mAh cm^{-2} and 82.12%). In the 2nd cycle, the reversible capacity of C_{Si}/GF cell is 1.25 mAh cm^{-2}, still larger than that of Csi/Cu cell (1.0 mAh cm^{-2}). Furthermore, we found the specific capacities of both cells are discrepant at different rates from 0.2 C to 5.0 C (Fig. 4b). Csi/GF cell at 0.2 C has higher capacity (558.5 mAh g^{-1}) than Csi/Cu cell (438.1 mAh g^{-1}), and the difference of capacities becomes obvious as the current density increases. The cell with GF shows steady discharge capacities, even though at high cycling rates. It displays capacities of 146.6 mAh g^{-1} at 2.0 C and 52.3 mAh g^{-1} at 5.0 C, higher than that of the cells with Cu foil (124.2 mAh g^{-1} at 2.0 C and 44.8 mAh g^{-1} at 5.0 C). These results demonstrate that GF performed the advantages of improving capacity and rate performance alternative Cu current collector at anode [51].

Next, we investigated the long cycle life of Csi/GF and Csi/Cu cells at a high rate of 2.0 C (Fig. 4c). The capacities show upward trend in first several cycles, which typically represents the electrochemical activation process. The stable capacity of Csi/Cu cell is about 101.35 mAh g^{-1} after 10 cycles, but degrades gradually to 58.77 mAh g^{-1} after 1000 cycles. By contrast, Csi/GF cell has the initial capacity of 142.31 mAh g^{-1} and good capacity retention with a capacity of 102.18 mAh g^{-1} after 1000 cycles. These results indicate excellent rate capability and cycling durability of cells with GF, and show promising possibility for its practical applications.

We also analyzed the mechanism of GF as current collect at anode. EIS results (Fig. S9) present a small ohmic resistance, indicating an excellent electrical contact between anode and current collect. Especially, the smaller Rct value of Csi/GF demonstrates a larger exchange current density compared with Csi/Cu. In addition, the charge/discharge curves (Fig. S10) of pure GF show an area capacity of ~0.3 mAh cm^{-2}, which increase the total capacity of anode and lowers the mass of C_{Si} when designing a battery with a certain capacity. The cross-sectional SEM images of GF (Fig. 4b) before and (Fig. 4c, Figs. S11 and S12) after cycling provide direct evidence of the lithium intercalation. Meanwhile, the adjustable spacing between the graphite sheets can relieve stress caused by the volume change of anode materials during charge/discharge [52], thus improving the cycle performance of LIBs. Therefore, we conclude that GF as current collector can enhance the specific storage and cycle life of anode for LIBs.

Full-cells were assembled with $LiCoO_2$ as cathode and C_{Si} as anode to demonstrate the practical applications of GF current collector. For comparison, we assembled four kinds of full cells: Al/$LiCoO_2$||Csi_i/Cu, Al/$LiCoO_2$||Csi/GF, GF/$LiCoO_2$||Csi/Cu and GF/$LiCoO_2$||Csi/GF. By comparing the discharge/charge curves, we found GF/$LiCoO_2$||Csi/GF shows the minimum polarization (Fig. 5a and Fig. S13). The cycling performance at 0.1 C shows a super stability at 1.0 mAh cm^{-2} of area capacity even though we changed the common current collector to GF (Fig. 5b and Fig. S14). After 100 cycles, the capacity retention of GF/$LiCoO_2$||Csi/GF full-cell is maintained at 97.54% with a CE of 99.92%, while for traditional Al/$LiCoO_2$||Csi/Cu full-cell, it is 94.74% of capacity retention with a CE of 99.83%. Furthermore, the relationship of area capacity and electrode energy density on different current collectors were illustrated (Fig. 5c). When the weight of all active materials and both current collectors are considered, the electrode energy density of GF/$LiCoO_2$||Csi/GF full-cell becomes higher than that of full cell using Al and Cu as current collector. Especially, as the area capacity of the electrode increases to standard 4 mAh cm^{-2} of commercial cells, the electrode energy density of GF/$LiCoO_2$||Csi/GF full-cell reaches 332 Wh kg^{-1}, while traditional Al/$LiCoO_2$||Csi/Cu only has an electrode energy

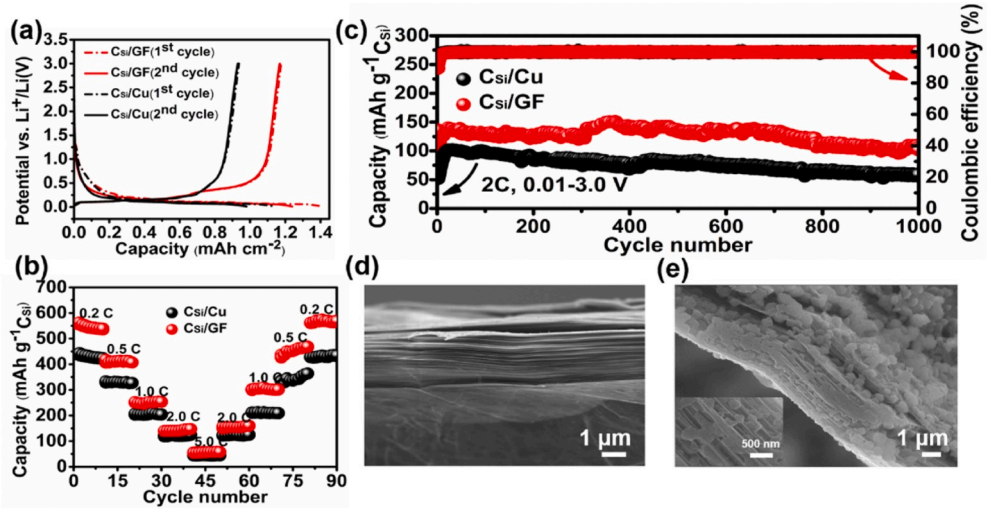

Fig. 4. (a) Initial 2 cycled discharge/charge curves at 0.1 C, (b) rate capability between 0.2 C and 5.0 C, and (c) cycling performance at 2.0 C of the commercial Csi anode on Cu foil and GF current collectors, (d, e) SEM images of GF before and after cycling, the insert image of (e) is partially enlarged image.

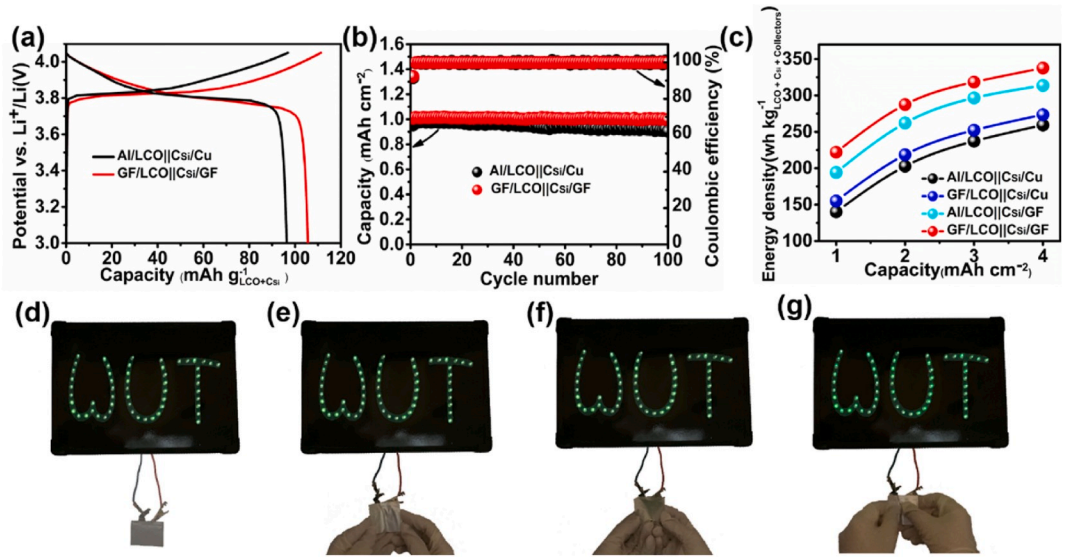

Fig. 5. Electrochemical Performance of full cells with GF or metal current collectors. (a) Galvanostatic discharge/charge curves at 0.1 C, (b) cycling performance at 0.1 C and (c) electrode energy density change with increasing area capacity of $LiCoO_2$||Csi full-cells with different current collector, (d–g) photographs of the flexible pouch cell powering a light-emitting diode board under various bending conditions.

density of 260 Wh kg^{-1}.

To further demonstrate the feasibility of GF for flexible electronic devices, flexible pouch cells were assembled with commercial $LiCoO_2$ cathode andCsi anode. After charging to 4.2 V, the flexible cell could stably power a light-emitting diode (LED) board, regardless of a series of large-angle bending and distorting (Fig. 5d-g and Video S1), demonstrating the superior conductivity and excellent mechanical stability, effectively promising its applications in flexible electronics.

Supplementary data related to this article can be found at https://doi.org/10.1016/j.jpowsour.2020.227991.

Based on the above results, the enhanced performances with graphite films as current collector can be explained as follows: (i) High electrical conductivity and excellent flexibility of graphite film guaranteed its feasibility of being used as current collector. (ii) Rough surface of graphite films provides larger contact area between electrode and current collectors, shortening the diffusion distance of lithium ions. (iii) Whether at high or low potentials, the graphite film can maintain the structure stability, and its certain elasticity can free more space for buffering volume changes during the cycles. (iiii) Most importantly, when replacing both cathode and anode collectors in full cells, the ultralight weight and extra Li-storage properties of graphite films lead to the obviously improved specific energy density of LIBs.

4. Conclusion

In summary, we have proposed an effective strategy to improve the specific energy density and mechanical performance of existing LIBs by means of the unique graphite film as current collectors. We successfully prepared graphite films through a simple and direct two steps heating approach, which showed ultra-lightweight (3.44 mg cm^{-2}), as well as highly conductive ($1.07*10^6$ S m^{-1}), anti-wrinkle and heat-sinking properties. As an attempt of their preliminary application, we favorably employed them in LIBs to replace the traditional metal current collectors (such as Al and Cu foils). As a result, it displayed outstanding cycling performance (142.31 mA h g^{-1} at 2.0C with a capacity retention of 71.80% after 1000 cycles in C_{Si} half-cell, showing 13.82% improvement than that using the Cu collector). For full cells, in addition to maintaining the same stable cycling performance as metal current collectors, the extremely light weight of graphite films also resulted in more than 25% improvement in electrode gravimetric energy density (332 Wh kg^{-1}) than that (260 Wh kg^{-1}) of $LiCoO_2$||Csi full-cell with Cu and Al current collectors. Moreover, the graphite film was used in flexible pouch cells with stable power output during various bending and distorting, which guarantees its desirable application in full flexible LIBs. Undoubtedly, the graphite film will be widely used in batteries and other devices in the future.

Declaration of competing interest

The authors declare that they have no known competing financial interests or personal relationships that could have appeared to influence the work reported in this paper.

CRediT authorship contribution statement

Qian Wu: Investigation, Methodology, Formal analysis, Writing - original draft, Writing - review & editing. **Jinlong Yang:** Investigation, Methodology, Formal analysis, Writing - original draft, Writing - review & editing. **Yuwei Zhao:** Investigation, Methodology, Writing - review & editing. **Rongguo Song:** Investigation, Methodology, Writing - review & editing. **Zhe Wang:** Investigation, Methodology, Writing - review & editing. **Zhe Huang:** Investigation, Methodology. **Mingyuan Shi:** Investigation, Methodology, Writing - review & editing. **Daping He:** Investigation, Methodology, Formal analysis, Writing - original draft, Writing - review & editing, Funding acquisition. **Shichun Mu:** Formal analysis, Writing - original draft, Writing - review & editing, Funding acquisition.

Acknowledgements

The research was financially supported by National Key Research and Development Program of China (No. 2016YFA0202603), National Natural Science Foundation of China (No. 51602009), International Postdoctoral Exchange Fellowship Program (No. 20170098) and 2018 National Key R&D Program of China 257.

Appendix A. Supplementary data

Supplementary data to this article can be found online at https://doi.org/10.1016/j.jpowsour.2020.227991.

References

[1] M. Armand, J.M. Tarascon, Nature 451 (2008) 652.
[2] E.J. Berg, C. Villevieille, D. Streich, S. Trabesinger, P. Novák, J. Electrochem. Soc. 162 (2015) A2468–A2475.
[3] H. Li, Z. Wang, L. Chen, X. Huang, Adv. Mater. 21 (2009) 4593–4607.
[4] Y.-K. Sun, Z. Chen, H.-J. Noh, D.-J. Lee, H.-G. Jung, Y. Ren, S. Wang, C.S. Yoon, S.-T. Myung, K. Amine, Nat. Mater. 11 (2012) 942.
[5] X.-L. Wu, Y.-G. Guo, J. Su, J.-W. Xiong, Y.-L. Zhang, L.-J. Wan, Adv. Energy Mater. 3 (2013) 1155–1160.
[6] D. Wang, I. Belharouak, G. Zhou, K. Amine, Adv. Funct. Mater. 23 (2013) 1070–1075.
[7] X. Zhang, I. Belharouak, L. Li, Y. Lei, J.W. Elam, A. Nie, X. Chen, R.S. Yassar, R. L. Axelbaum, Adv. Energy Mater. 3 (2013) 1299–1307.
[8] S. Lee, Y. Cho, H.-K. Song, K.T. Lee, J. Cho, Angew. Chem. Int. Ed. 51 (2012) 8748–8752.
[9] D. Gu, W. Li, F. Wang, H. Bongard, B. Spliethoff, W. Schmidt, C. Weidenthaler, Y. Xia, D. Zhao, F. Schüth, Angew. Chem. Int. Ed. 54 (2015) 7060–7064.
[10] I.H. Son, J. Hwan Park, S. Kwon, S. Park, M.H. Rümmeli, A. Bachmatiuk, H.J. Song, J. Ku, J.W. Choi, J.-m. Choi, S.-G. Doo, H. Chang, Nat. Commun. 6 (2015) 7393.
[11] K. Mizushima, P.C. Jones, P.J. Wiseman, J.B. Goodenough, Mater. Res. Bull. 15 (1980) 783–789.
[12] P. Liu, H. Zhang, W. He, T. Xiong, Y. Cheng, Q. Xie, Y. Ma, H. Zheng, L. Wang, Z.-Z. Zhu, Y. Peng, L. Mai, D.-L. Peng, J. Am. Chem. Soc. 141 (2019) 10876–10882.
[13] Z. Huang, T. Xiong, X. Lin, M. Tian, W. Zeng, J. He, M. Shi, J. Li, G. Zhang, L. Mai, S. Mu, J. Power Sources 432 (2019) 8–15.
[14] B.A. Johnson, R.E. White, J. Power Sources 70 (1998) 48–54.
[15] P.L. Taberna, S. Mitra, P. Poizot, P. Simon, J.M. Tarascon, Nat. Mater. 5 (2006) 567–573.
[16] M. Yao, K. Okuno, T. Iwaki, M. Kato, S. Tanase, K. Emura, T. Sakai, J. Power Sources 173 (2007) 545–549.
[17] Y.-L. Kim, Y.-K. Sun, S.-M. Lee, Electrochim. Acta 53 (2008) 4500–4504.
[18] C. Wang, J. Xu, R. Ma, M.-F. Yuen, Mater. Chem. Phys. 148 (2014) 411–415.
[19] K.R. Adair, C. Zhao, M.N. Banis, Y. Zhao, R. Li, M. Cai, X. Sun, Angew. Chem. Int. Ed. 58 (2019) 15797–15802.
[20] Z.e. Xiao, J. Chen, J. Liu, T. Liang, Y. Xu, C. Zhu, S. Zhong, J. Power Sources 438 (2019) 226973.
[21] Z. Yi, N. Lin, Y. Zhao, W. Wang, Y. Qian, Y. Zhu, Y. Qian, Energy Storage Mater 17 (2019) 93–100.
[22] Y. Chen, K. Fu, S. Zhu, W. Luo, Y. Wang, Y. Li, E. Hitz, Y. Yao, J. Dai, J. Wan, V. A. Danner, T. Li, L. Hu, Nano Lett. 16 (2016) 3616–3623.
[23] A.L.M. Reddy, A. Srivastava, S.R. Gowda, H. Gullapalli, M. Dubey, P.M. Ajayan, ACS Nano 4 (2010) 6337–6342.
[24] R. Zhou, C. Meng, F. Zhu, Q. Li, C. Liu, S. Fan, K. Jiang, Nanotechnology 21 (2010) 345701.
[25] L. Hu, H. Wu, F. La Mantia, Y. Yang, Y. Cui, ACS Nano 4 (2010) 5843–5848.
[26] L. Wang, X. He, J. Li, J. Gao, M. Fang, G. Tian, J. Wang, S. Fan, J. Power Sources 239 (2013) 623–627.
[27] J. Zhao, S. Pei, W. Ren, L. Gao, H.-M. Cheng, ACS Nano 4 (2010) 5245–5252.
[28] D. Li, M.B. Müller, S. Gilje, R.B. Kaner, G.G. Wallace, Nat. Nanotechnol. 3 (2008) 101.
[29] H. Chen, M.B. Müller, K.J. Gilmore, G.G. Wallace, D. Li, Adv. Mater. 20 (2008) 3557–3561.
[30] R. Cruz-Silva, A. Morelos-Gomez, H.-i. Kim, H.-k. Jang, F. Tristan, S. Vega-Diaz, L. P. Rajukumar, A.L. Elías, N. Perea-Lopez, J. Suhr, M. Endo, M. Terrones, ACS Nano 8 (2014) 5959–5967.
[31] X. Wang, L. Zhi, K. Müllen, Nano Lett. 8 (2008) 323–327.
[32] S. Pei, H.-M. Cheng, Carbon 50 (2012) 3210–3228.
[33] Q. Su, S. Pang, V. Alijani, C. Li, X. Feng, K. Müllen, Adv. Mater. 21 (2009) 3191–3195.
[34] G. Xin, T. Yao, H. Sun, S.M. Scott, D. Shao, G. Wang, J. Lian, Science 349 (2015) 1083.
[35] M. Murakami, N. Nishiki, K. Nakamura, J. Ehara, H. Okada, T. Kouzaki, K. Watanabe, T. Hoshi, S. Yoshimura, Carbon 30 (1992) 255–262.
[36] S. Chen, C. Niu, H. Lee, Q. Li, L. Yu, W. Xu, J.-G. Zhang, E.J. Dufek, M. S. Whittingham, S. Meng, J. Xiao, J. Liu, Joule 3 (2019) 1094–1105.
[37] A. Barreiro, F. Börrnert, S.M. Avdoshenko, B. Rellinghaus, G. Cuniberti, M. H. Rümmeli, L.M.K. Vandersypen, Sci. Rep. 3 (2013) 1115.
[38] A. Barreiro, F. Börrnert, M.H. Rümmeli, B. Büchner, L.M.K. Vandersypen, Nano Lett. 12 (2012) 1873–1878.
[39] B. Shen, W. Zhai, W. Zheng, Adv. Funct. Mater. 24 (2014) 4542–4548.
[40] N. Wu, W. Du, X. Gao, L. Zhao, G. Liu, X. Liu, H. Wu, Y.-B. He, Nanoscale 10 (2018) 11460–11466.
[41] Z. Zhang, L. Wang, Y. Li, Y. Wang, J. Zhang, G. Guan, Z. Pan, G. Zheng, H. Peng, Adv. Energy Mater. 7 (2017) 1601814.
[42] W.J. Lee, J. Lim, S.O. Kim, Small Methods 1 (2017) 1600014.
[43] Y. Zhu, J. Xie, A. Pei, B. Liu, Y. Wu, D. Lin, J. Li, H. Wang, H. Chen, J. Xu, A. Yang, C.-L. Wu, H. Wang, W. Chen, Y. Cui, Nat. Commun. 10 (2019) 2067.
[44] J. Yang, X. Kang, L. Hu, X. Gong, S. Mu, J. Mater. Chem. 2 (2014) 6870–6878.
[45] R. Fu, Y. Li, H. Yang, Y. Zhang, X. Cheng, J. Electrochem. Soc. 160 (2013) A3048–A3053.
[46] Y. Tsuchiya, M. Yoshiki, J. Koga, A. Nishiyama, M. Koyama, M. Ogawa, S. Zaima, IEEE Trans. Electron. Dev. 55 (2008) 2648–2656.
[47] T. Kawai, K. Tanimura, T. Sakata, Chem. Phys. Lett. 56 (1978) 541–545.
[48] P. Liu, Y. Wei, K. Jiang, Q. Sun, X. Zhang, S. Fan, S. Zhang, C. Ning, J. Deng, Phys. Rev. B 73 (2006) 235412.
[49] T.J. Fabish, M.L. Hair, J. Colloid Interface Sci. 62 (1977) 16–23.
[50] J. Yang, X. Kang, L. Hu, X. Gong, D. He, T. Peng, S. Mu, J. Alloys Compd. 572 (2013) 158–162.
[51] M.S. Yazici, D. Krassowski, J. Prakash, J. Power Sources 141 (2005) 171–176.
[52] Y. Song, Z. Li, J. Zhang, J. Power Sources 263 (2014) 22–28.